Gradient and scattering forces in photoinduced force microscopy

Junghoon Jahng,[1] Jordan Brocious,[1] Dmitry A. Fishman,[2] Fei Huang,[3] Xiaowei Li,[2] Venkata Ananth Tamma,[2] H. Kumar Wickramasinghe,[3] and Eric Olaf Potma[2,*]

[1]*Department of Physics and Astronomy, University of California, Irvine, California 92697, USA*

[2]*Department of Chemistry, University of California, Irvine, California 92697, USA*

[3]*Department of Electrical Engineering and Computer Science, University of California, Irvine, California 92697, USA*

(Received 28 July 2014; revised manuscript received 22 September 2014; published 10 October 2014)

A theoretical and experimental analysis of the dominant forces measured in photoinduced force microscopy is presented. It is shown that when operated in the noncontact and soft-contact modes, the microscope is sensitive to the optically induced gradient force (F_g) and the scattering force (F_{sc}). The reconstructed force-distance curve reveals a tip-dependent scattering force in the 30–60 pN range. Whereas the scattering force is virtually insensitive to the nanoscopic tip-sample distance, the gradient force shows a z^{-4} dependence and is manifest only for tip-sample distances of a few nm. Measurements on glass, gold nanowires, and molecular clusters of silicon naphtalocyanine confirm that the gradient force is strongly dependent on the polarizability of the sample, enabling spectroscopic imaging through force detection. The nearly constant F_{sc} and the spatially dependent F_g give rise to a complex force-distance curve, which varies from point to point in the specimen and dictates the image contrast observed for a given set point of the cantilevered tip.

DOI: 10.1103/PhysRevB.90.155417 PACS number(s): 68.37.Ps, 07.79.Lh

I. INTRODUCTION

Atomic force microscopy (AFM) generates images based on variations in the local forces between an atomic tip and the surface specimen. The nanoscopic resolution provided by AFM yields topographic images with exquisite detail, enabling visualization of individual atoms and intermolecular bonds under optimized conditions [1,2]. Although the contrast in AFM is primarily topographic in nature, chemical information about the sample can be obtained by exploiting specific chemical interactions that may exist in the tip-sample junction [3,4]. Another form of chemical selectively can be obtained by combining force microscopy with the analytical capabilities offered through optical spectroscopy.

Dressing the atomic force microscope with spectroscopic sensitivity is attractive, as it would allow various forms of molecular spectroscopy to be carried out at high spatial resolution. A successful example in this category of techniques is infrared (IR) absorption AFM, also referred to as the photothermal-induced resonance technique [5–8]. In this technique, the sample is illuminated with infrared light, giving rise to heating of the material through direct excitation of dipole allowed vibrational transitions. The thermal expansion that follows is selective to spectroscopic transitions and can be probed with high spatial resolution through contact-mode AFM [9]. IR-based AFM has been used successfully to visualize molecular layers on surfaces with chemical selectivity and with a spatial resolution down to 25 nm [8].

An alternative method is photoinduced force microscopy (PIFM), which probes the optically induced changes in the dipolar interactions between a sharp polarizable tip and the sample [10,11]. Unlike IR-AFM, the contrast in PIFM does not rely on the thermal expansion of the material. Rather, the technique is directly sensitive to the electromagnetic forces at play in the tip-sample junction, and can, in principle, be conducted in noncontact-mode AFM. The advantage of this approach is that optical transitions can be probed directly, as dissipation of excitation energy in the material is not required for generating contrast. In addition, the photoinduced forces are spatially confined and fundamentally decoupled from heat diffusion, giving rise to a high spatial resolution of 10 nm or better [11]. Theoretically, the spectroscopic information probed in this technique is akin to information accessible through coherent optical spectroscopy with heterodyne detection [12]. PIFM has been successfully demonstrated through linear excitation of dipole-allowed electronic transitions [10] as well as nonlinear excitation of Raman-active transitions [11].

Although PIFM is a promising technique, the current theoretical understanding of the relevant forces in the tip-sample junction is rudimentary at best. In this contribution, we provide a simple description of the operating principle of the photoinduced force microscope in terms of classical fields and forces. By including both the attractive gradient interactions and the repulsive scattering force, we simulate the characteristics of the force-distance curve and compare the predicted profile with experimental results obtained from gold nanowires and molecular nanoclusters. Our study identifies the distance regimes in which attractive gradient forces are dominant and points out under which conditions molecular selective signals are optimized. Finally, our experiments show that the technique can be carried out in the femtosecond illumination mode, paving the way for more advanced nonlinear optical investigations at the nanoscale level.

II. THEORETICAL DESCRIPTION OF PHOTOINDUCED FORCE MICROSCOPY

A. Time-averaged Lorentz force

We consider a monochromatic electromagnetic wave with angular frequency ω, which is incident on a polarizable

*Corresponding author: epotma@uci.edu

particle. The time harmonic electric and magnetic field components at location **r** can be written as

$$\mathbf{E}(\mathbf{r},t) = \mathrm{Re}\{\mathbf{E}(\mathbf{r})e^{-i\omega t}\}, \tag{1}$$

$$\mathbf{B}(\mathbf{r},t) = \mathrm{Re}\{\mathbf{B}(\mathbf{r})e^{-i\omega t}\}. \tag{2}$$

To the first order in the fields, the induced dipole moment of the particle assumes the same time dependence and is given as

$$\vec{\mu}(\mathbf{r},t) = \mathrm{Re}\{\vec{\mu}(\mathbf{r})e^{-i\omega t}\}.$$

We assume that the particle has no static dipole moment. In this case, to the first order, the induced dipole moment is proportional to the electric field at the particle's position **r**:

$$\vec{\mu}(\mathbf{r}) = \alpha(\omega)\mathbf{E}(\mathbf{r}), \tag{3}$$

where α denotes the polarizability of a particle that satisfies the Clausius-Mossotti equation

$$\alpha = 4\pi\epsilon_0\left(\frac{\epsilon-1}{\epsilon+2}\right)a^3, \tag{4}$$

where a is the particle radius and ϵ denotes the complex dielectric permittivity. Generally, α is a tensor of rank two, but for atoms and molecules it is legitimate to use a scalar representation since only the projection of $\vec{\mu}$ along the direction of the electric field is of direct relevance.

Using the dipole approximation for calculating the force between tip and molecule, the cycle-averaged Lorentz force is [13]

$$\langle\mathbf{F}\rangle = \frac{\alpha'}{2}\nabla\langle|\mathbf{E}|^2\rangle + \omega\alpha''\langle\mathbf{E}\times\mathbf{B}\rangle, \tag{5}$$

where α' is a real part of a particle polarizability and α'' is an imaginary part of a particle polarizability that satisfies $\alpha(\omega) = \alpha'(\omega) + i\alpha''(\omega)$. The first term of Eq. (5) is recognized as the gradient force (or dipole force) and the second term is denoted the scattering or absorption force. The gradient force originates from field inhomogeneities, and is proportional to the dispersive part (real part) of the complex polarizability. On the other hand, the scattering or absorption force is proportional to the dissipative part (imaginary part) of the complex polarizability.

Equation (5) is a good description of the force if it can be assumed that the field between the particle and the tip dipoles varies slowly [13]. This assumption is generally valid if the particle does not substantially change the spatial properties of the incident field, as is the case in the point-dipole approximation. In the case of the gradient force, it has been shown that the assumption of a slowly varying field produces acceptable results even when particle and tip dimensions approach the 10 nm range [13]. Such a spatial scale pertains to our experiments as well. Therefore, we assume that Eq. (5) is a valid expression for predicting the general trends of the photoinduced force as relevant to typical PIFM measurements.

B. Gradient force

The photoinduced gradient force between tip and sample is a mutual interaction force. The electric field experienced by the sample particle (molecule) is a combination of the incident electric field and the evanescent field of the induced dipole in the tip, and vice versa. The mutual interaction can be modeled by considering both the tip and molecule as spherical particles of volume $\frac{4\pi}{3}a^3$ and an effective polarizability α. In this description, the induced dipole moments in each of the particles are

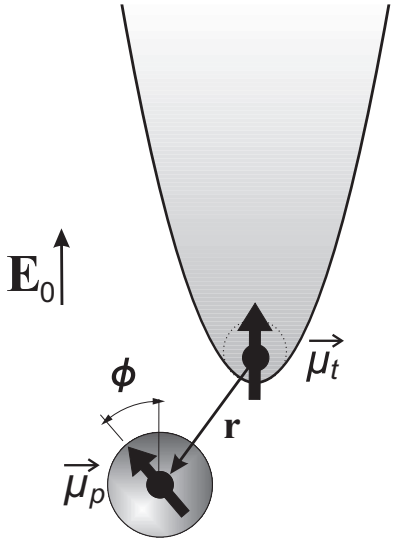

FIG. 1. Graphical representation of the symbols used to derive the mechanical force in the dipolar limit. **r** denotes the center-of-mass coordinate.

$$\vec{\mu}_t = \alpha_t(\mathbf{E}_0 + \mathbf{E}_p), \tag{6}$$

$$\vec{\mu}_p = \alpha_p(\mathbf{E}_0 + \mathbf{E}_t), \tag{7}$$

where $\mathbf{E}_0$ is the electric field of the incident laser, and $\vec{\mu}_t$ and $\vec{\mu}_p$ are the effective dipole moments of the tip and molecule, respectively. $\mathbf{E}_t$ and $\mathbf{E}_p$ are the evanescent electric fields of the tip and molecule, respectively. For our discussion here, the forces in the z dimension dominate the cantilever response (see Figs. 1 and 2). We therefore consider $\vec{\mu}_t = \mu_t\hat{z}$ and $\vec{\mu}_p = \mu_p\hat{z}$, the z components of the dipole moment of the tip and molecule. Then the static electric fields of the induced dipoles are

$$\mathbf{E}_i = \frac{1}{4\pi\varepsilon_0}\frac{(3\vec{\mu}_i\cdot\mathbf{r})\mathbf{r} - \vec{\mu}_i}{r^3}, \tag{8}$$

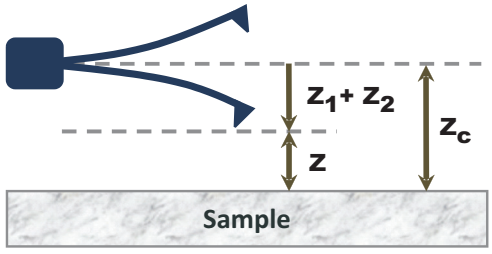

FIG. 2. (Color online) Graphical representation of the cantilever motion. z is the instantaneous position of cantilever. z_c is the average position, z_1 is the oscillation of the fundamental resonance, and z_2 is the oscillation of the higher-order resonance.

where $\mathbf{E}_i = E_{ix}\hat{x} + E_{iy}\hat{y} + E_{iz}\hat{z}$, $r = \sqrt{x^2+y^2+z^2}$, and $i = t, p$ respectively. Because of the azimuthal symmetry, E_{ix} is similar to E_{iy}. Using (6)–(8), the z component of the molecule's dipole moment and its corresponding electric field $\mathbf{E}_p$ can be found as

$$\mu_p = \frac{2z^3\pi\alpha_p\varepsilon_0(\alpha_t + 2z^3\pi\varepsilon_0)E_{0z}}{4z^6\pi^2\varepsilon_0^2 - \alpha_p\alpha_t}, \tag{9}$$

$$E_{p_z} = \frac{\alpha_p(\alpha_t + 2z^3\pi\varepsilon_0)E_{0z}}{4z^6\pi^2\varepsilon_0^2 - \alpha_p\alpha_t}, \tag{10}$$

with $\mathbf{E}_0 = E_{0x}\hat{x} + E_{0y}\hat{y} + E_{0z}\hat{z}$. The expressions (9) and (10) can be simplified when it is assumed that the distance between the tip and molecule is larger than the physical size of the particles, i.e., $z > a_t$ and $z > a_p$. Because the polarizabilities of the tip and molecule scale with the cube of the particle radius, as in (4), we may also write $z^6 \gg a_p^3 a_t^3$. Under these reasonable assumptions, the z component of the gradient force is reduced to

$$F_g \equiv \langle \mathbf{F}_g \rangle_z \simeq -\frac{3\alpha_p'\alpha_t'}{2\pi z^4} E_{0z}^2. \tag{11}$$

We see from (11) that the optically induced gradient force exhibits a z^{-4} dependence. It is thus a force that is expected to be prominent in only a narrow nanoscopic range of the tip-molecule distance, and less relevant for larger separations of molecule and tip. The negative sign in this interaction indicates that the force is attractive. Note that the strength of the force depends on the polarizability α_p of the sample particle. The expression in (11) is similar to the formula previously used in [10]. We will use the parameter $\beta = 3\alpha_p'\alpha_t' E_{0z}^2/2\pi$ to characterize the magnitude of the gradient force in a given measurement.

C. Scattering force

Besides the attractive gradient force, Eq. (5) predicts another optically induced force. This second contribution is recognized as the scattering force, which is generally repulsive. The magnitude of the scattering force is proportional to the dissipative part of the interaction of light with the polarizable particles, as described by the imaginary part of the complex polarizability. From Eq. (5), the scattering force can be described as

$$F_{sc} \equiv \langle \mathbf{F}_{sc} \rangle_z = \omega\alpha_t'' \langle \mathbf{E}_0 \times \mathbf{B}_0 \rangle_z, \tag{12}$$

where $\mathbf{B}_0 = B_{0x}\hat{x} + B_{0y}\hat{y} + B_{0z}\hat{z}$. Only the transverse electric and magnetic field components contribute to the the force along the z direction. Given that the dominant component of the incident field is polarized along x, i.e., $\mathbf{E_0} \approx E_{0x}\hat{x}$, the absorption force can be written as

$$\langle \mathbf{F}_{sc} \rangle_z = \frac{2\pi\alpha_t''}{\lambda} E_{0x}^2, \tag{13}$$

where λ is the wavelength of the incident beam. Unlike the gradient force, the scattering force is repulsive. In addition, whereas the gradient force is expected to scale as z^{-4} with tip-sample distance, the distance dependence of the scattering force is implicitly contained in the spatial extent of the excitation field E_{0x}. Because the axial dimension of the excitation field is in the (sub-)μm range, the scattering force manifests itself over a different spatial scale than the local gradient force. We expect, therefore, that the short-range nanoscopic interactions are governed by the gradient force, while at longer distances the scattering force is dominant. Note that the magnitude of the total photoinduced force may exhibit a minimum at the tip-sample distance where the attractive gradient force and the repulsive scattering force cancel.

D. Cantilever dynamics

We next consider the dynamics of the cantilever-tip system in the presence of the optically induced force $F_{\text{opt}} = F_g + F_{sc}$. The cantilever motion is modeled as a simple collection of independent point-mass harmonic oscillators, with motion confined to the z coordinate only. In practice, two mechanical resonances are of relevance to the photoinduced force microscopy experiment, namely the first- and a higher-order mechanical eigenmode of the cantilever-tip system. The first mechanical resonance is excited by the external driving force F_1 with frequency ω_1, whereas the higher-order resonance at ω_n is actively driven by F_{opt}. In addition, the cantilever tip is subject to the interaction force F_{int}, which includes all relevant van der Waals, electrostatic, magnetic, chemical, and Casimir forces, as well as average (unmodulated) optical forces. In this model, the equations of motion for the displacement of the first- (z_1) and higher-order (z_n) mode are found as

$$m\ddot{z}_1 + b_1\dot{z}_1 + k_1 z_1 = F_1\cos(\omega_1 t) + F_{\text{int}}(z(t)), \tag{14}$$

$$m\ddot{z}_n + b_n\dot{z}_n + k_n z_n = F_{\text{opt}}(z(t))\cos(\omega_n t) + F_{\text{int}}(z(t)), \tag{15}$$

where m is the effective mass of the cantilever; k_i and b_i are, respectively, the force constant and the damping coefficient of the ith eigenmode [14]. In the following, we will set $n = 2$, corresponding to the tip displacement of the second mechanical resonance, but the analysis applies equally to higher-order modes. Note that the resonance frequency ω_i and the external driving force F_1 can be expressed as $\omega_i = \sqrt{k_i/m}$ and $F_1 = k_1 A_{01}/Q_1$, respectively, where A_{01} is the free oscillation amplitude of the driven first eigenmode of the cantilever, and Q_i is the quality factor of the ith eigenmode. In addition, the damping coefficient can be expressed as $b_i = m\omega_i/Q_i$. The instantaneous tip-surface distance is represented by

$$\begin{aligned} z(t) &= z_c + z_1(t) + z_2(t) + O(\varepsilon) \\ &\approx z_c + A_1\sin(\omega_1 t + \theta_1) + A_2\sin(\omega_2 t + \theta_2), \end{aligned} \tag{16}$$

where z_c is the equilibrium position of the cantilever, A_i is the amplitude and θ_i is the phase shift of the ith eigenmode, and $O(\varepsilon)$ is a term that carries the contribution of the other modes and harmonics. Substituting Eq. (16) into Eqs. (14) and (15) by multiplying both sides of the resulting equation by $\sin(\omega_i t + \theta_i)$ and $\cos(\omega_i t + \theta_i)$, followed by an integration over the oscillation period, the following general relations for amplitude, phase, mechanical interaction force, and

photoinduced force are obtained:

$$\left(k_1 - m{\omega_1}^2\right)\frac{A_1}{2} = \frac{F_1}{2}\sin\theta_1 + \int_0^T F_{\text{int}}\sin(\omega_1 t + \theta_1)dt, \tag{17}$$

$$\frac{b_1\omega_1 A_1}{2} = \frac{F_1}{2}\cos\theta_1 + \int_0^T F_{\text{int}}\cos(\omega_1 t + \theta_1)dt, \tag{18}$$

$$\left(k_2 - m{\omega_2}^2\right)\frac{A_2}{2} = \int_0^T [F_{\text{int}} + F_{\text{opt}}\cos(\omega_2 t)]\sin(\omega_2 t + \theta_2)dt, \tag{19}$$

$$\frac{b_2\omega_2 A_2}{2} = \int_0^T [F_{\text{int}} + F_{\text{opt}}\cos(\omega_2 t)]\cos(\omega_2 t + \theta_2)dt. \tag{20}$$

If the form of F_{int} and F_{opt} is known, the amplitudes A_1, A_2 and the phase shifts θ_1, θ_2 can be calculated through numerical integration of Eqs. (17)–(20).

E. Reconstruction of distance-dependent force

The amplitude and phase of the first and second resonances are experimentally accessible quantities. We next describe an approximate method to relate the forces active at the tip-sample junction to these experimental quantities. In general, F_{int} is a nonlinear function of the tip-sample distance z and contains both conservative and dissipative (i.e., nonconservative) forces,

$$F_{\text{int}} = F_c(z) + F_{nc}, \tag{21}$$

where the conservative term F_c, by definition, depends only on the distance z. For our description here, we assume that the nonconservative force can be written as $F_{nc} = -\Gamma(z)\dot{z}$, where Γ represents the effective damping coefficient of a given dissipative interaction. Such a form of force describes many physical interactions that give rise to an energy loss of the cantilever movement [15–17]. Note that although the term $-\Gamma(z)\dot{z}$ may be replaced by some other specific forms of dissipation, one can still employ the effective and intuitive coefficient Γ as a parameter describing a given dissipation [18,19].

We use two approximations to simplify the description. First, we assume that the tip displacement is small such that the force at z can be obtained through a Taylor expansion of the force at the equilibrium position z_c [20]. Under these conditions, the mechanical interaction force and the photoinduced force can be expressed by

$$\begin{aligned} F_{\text{int}}(z(t)) &= F_c(z) - \Gamma(z)\dot{z} \\ &\approx F_c(z_c) + \left.\frac{\partial F_c(z)}{\partial z}\right|_{z_c}(z - z_c) - \Gamma(z_c)\dot{z}, \end{aligned} \tag{22}$$

$$F_{\text{opt}}(z(t)) \approx F_{\text{opt}}(z_c) + \left.\frac{\partial F_{\text{opt}}}{\partial z}\right|_{z_c}(z - z_c). \tag{23}$$

Second, we assume that the frequency of the first and second mechanical resonance are related as $\omega_2 \approx 6\omega_1$. In practice, the frequency of the second resonance is $6.27\omega_1$ [14]. Although the approximation $\omega_2 \approx 6\omega_1$ gives rise to numerical differences in the integration of Eqs. (17)–(20), this difference is small while the general physics of the problem remains preserved. Using the approximation $\omega_2 \approx 6\omega_1$, the forces are simplified to

$$F_c(z) = \int_z^\infty \left[\frac{F_1}{A_1(z)}\sin\theta_1(z) - \left(k_1 - m\omega_1^2\right)\right]dz, \tag{24}$$

$$\Gamma(z) = \frac{F_1}{A_1(z)\omega_1}\cos\theta_1(z) - b_1, \tag{25}$$

$$|F_{\text{opt}}(z)| = A_2(z)\sqrt{m^2\left(\omega'^2_2 - \omega_2^2\right)^2 + b'^2_2\omega_2^2}, \tag{26}$$

with

$$\begin{aligned} \omega'_2 &= \sqrt{\left(k_2 - \left.\frac{\partial F_c}{\partial z}\right|_z\right)\Big/ m}, \\ b'_2 &= b_2 - \Gamma(z). \end{aligned} \tag{27}$$

The formalism outlined by Eqs. (24)–(26) makes it possible to reconstruct the distance-dependent mechanical and photoinduced force from experimentally accessible parameters.

III. EXPERIMENTAL METHODS

A. Light source

The reported experiments are carried out with a femtosecond light source. The pulsed light is derived from a ti:sapphire laser (MaiTai, Spectra-Physics), which delivers 200 fs pulses with a center wavelength of 809 nm. The pulse repetition rate is 80 MHz and the average power of the laser beam at the sample plane is between 60 μW and 92 μW, depending on the experiment. The laser light is precompressed with a prism compressor to account for dispersion in the microscope optics. In addition, the laser light is amplitude modulated at a frequency that coincides with a higher-order mechanical resonance of the cantilever used in the experiment, as indicated below.

B. Atomic force microscope

A custom-modified atomic force microscope (Molecular Vista) is used for the photoinduced force experiments. A simplified scheme is given in Fig. 3. The system consists of an inverted optical microscope outfitted with an NA = 1.40 oil immersion objective, a sample stage scanner, an AFM scan head, and transmission and reflection optics for sample inspection. The microscope objective generates a diffraction-limited focal spot at the sample surface using x-polarized laser light. In the focal plane, significant portions of y-polarized and z-polarized light are present, which have distinct focal field distributions. The tip is positioned at the location of maximum z-polarized light [21] to enhance the sensitivity of the measurement to the z-directed gradient forces.

A 30 nm radius gold coated silicon tip is used in the experiments (FORTGG, AppNano). Two cantilever systems are employed. The first cantilever system has $k_1 = 1.61$ N/m, $Q_1 = 181.93$, and a first mechanical resonance $f_{01} = 58.73$ kHz. The second mechanical resonance of the cantilever is at $f_{02} = 372.41$ kHz, with $k_2 = 52.24$ N/m and $Q_2 = 561.36$. The free oscillation amplitude of the fundamental resonance A_{01} is set to 38 nm in the experiments below. The laser modulation frequency was set to 372.41 kHz

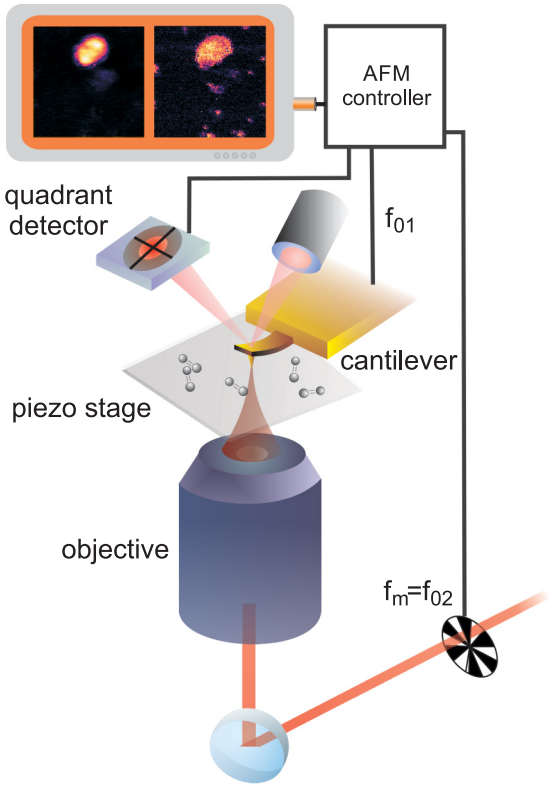

FIG. 3. (Color online) Sketch of the photoinduced force microscope.

for photoinduced force measurements, coinciding with the second mechanical resonance of the cantilever. The second cantilever system exhibits a mechanical resonance at $f_{01} = 58.58$ kHz with $k_1 = 1.6$ N/m and $Q_1 = 178$, operated with a free oscillation amplitude $A_{01} = 41$ nm. The photoinduced force measurements with this system are carried out at the third mechanical resonance of the cantilever, which is found at $f_{03} = 1033.190$ kHz. The corresponding spring constant and quality factor of this resonance are $k_3 = 492.51$ N/m and $Q_3 = 539$, respectively.

The topographic and PIFM images are acquired simultaneously. This is achieved by demodulating the tip response at f_{01} to retrieve the topography image and at f_{02} (or f_{03}) to retrieve the photoinduced force image. The AFM controller of the Molecular Vista system includes a digital lock-in amplifier, used for demodulation of the signals, and a digital function generation with a field programmable gate array (FPGA), used for generating synchronized clock signals.

C. Sample materials

Two test samples are used in this study. The first sample is a composed of a 0.17 mm thick borosilicate coverslip with deposited gold nanowires. The nanowires are fabricated by the lithographically patterned nanowire electrodeposition technique [22]. The resulting nanowires feature an average width of 120 nm and an average height of 25 nm, whereas the length of the nanowires extends over millimeters. The second sample is a borosilicate coverslip with deposited nanoclusters of silicon naphtalocyanine (SiNc). The samples are prepared by spin-casting a concentrated solution of SiNc in toluene onto the plasma-cleaned coverslip. After evaporation of the solvent, nanoscale aggregates of SiNc are formed, varying in size from several micrometers to less than 10 nm in diameter.

IV. RESULTS AND DISCUSSION

A. Force-distance simulations

We first study the general trends of the cantilever dynamics in the presence of both mechanical and photoinduced forces using Eqs. (17)–(20). For this purpose, it is required to choose a functional form of the forces $F_{\rm int}$ and $F_{\rm opt}$ that are active at the tip-sample junction. We assume that $F_{\rm int}$ is described by a conservative Lennard-Jones-type force that contains a $1/z^6$ (repulsive) and a $1/z^2$ (attractive) force term,

$$F_{\rm int} = f_0\left(\frac{l^4}{3z^6} - \frac{1}{z^2}\right), \tag{28}$$

where f_0 is a constant and l is the characteristic distance at which the attractive force is minimized. For $F_{\rm opt}$ we obtain from Eqs. (11) and (13)

$$F_{\rm opt} = -\frac{3\alpha_t'\alpha_p'}{2\pi z^4}E_{0z}^2 + \frac{2\pi\alpha_t''}{\lambda}E_{0x}^2. \tag{29}$$

Figure 4 shows the distance-dependent amplitude (a) and the phase (b) of the first resonance, as well as the amplitude of second resonance (c) as simulated with Eqs. (17)–(20) and the chosen forces above. The z-dependent amplitude and phase of the first resonance show the expected profile for the chosen form of $F_{\rm int}$. The amplitude of the second resonance, on the other hand, displays a very different profile, depicted by the black curve in Fig. 4(c). A peak near $z \approx 11$ nm is seen, the amplitude of which is dependent on the magnitude of the effective polarizability. Around $z \approx 15$ nm a sharp dip is observed, followed by a plateau at longer distances. Unlike the first resonance, the second resonance is sensitive to the presence of $F_{\rm opt}$. The characteristic shape of the amplitude-distance curve reflects the presence of both the attractive gradient force and the repulsive scattering force. At shorter distances, the gradient force dominates, whereas for longer tip-sample separations the response is governed by the scattering force. The dip appears when the two optical forces cancel, i.e., $F_g + F_{sc} = 0$.

The red curve in Fig. 4(c) is obtained by increasing the magnitude of F_g by a factor of 2; i.e., β is twice as large as for the black curve, whereas F_{sc} remains the same. Two immediate changes are observed. First, the maximum amplitude A_2 is significantly larger for the 2β case, as can be expected for an increase in the magnitude of the gradient force. Second, the cancellation of the two optical forces now occurs at a longer distance, near ~18 nm rather than near ~15 nm in this simulation. An increase in the gradient force thus gives rise to an amplitude-distance curve that appears shifted to longer distances.

The formalism outlined in Eqs. (24)–(26) can be used to reconstruct the mechanical and photoinduced forces between the tip and sample from the simulated amplitude-distance curves. The black solid line in Fig. 4(d) represents the functional form of the assumed mechanical force, as given

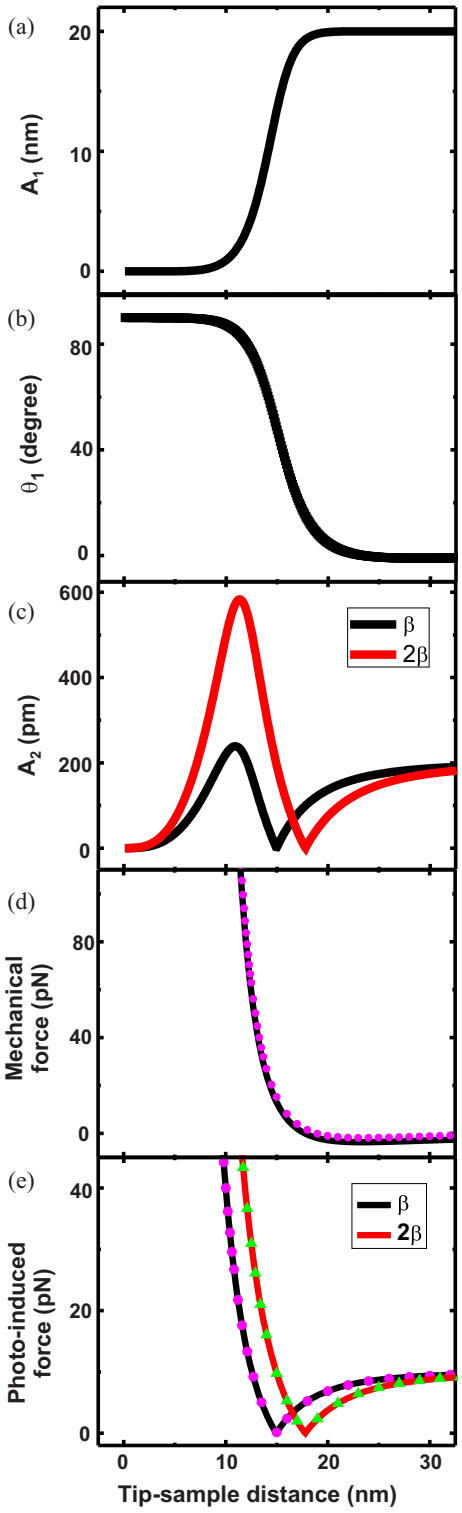

FIG. 4. (Color online) Simulation of the amplitude-distance curve (a) and the phase-distance curve (b) of the fundamental resonance of a cantilever. The free oscillation amplitude of A_{01} is 20 nm. (c) Amplitude-distance curve of the second resonance of the cantilever for F_g with β (black) and 2β (red). (d) Pre-assumed Lennard-Jones-type force (solid black) and the reconstructed force (purple dots). (e) Pre-assumed total magnitude of the optical force for β (solid black) and 2β (solid red), along with the corresponding reconstructed forces for β (purple dots) and 2β (green triangle). The experimental parameters of the simulation are given in [23].

by Eq. (28). The purple dots indicate the reconstructed force from the simulated measurement. The close correspondence between the assumed and reconstructed data indicates that the assumptions made in (24)–(26) are justified. Similarly, the solid black line in Fig. 4(e) shows the chosen form of the photoinduced force, described by Eq. (29), whereas the purple dots correspond to the reconstructed data. The simulated experiments presented in Fig. 4 underline that the photoinduced force can be extracted from measured amplitude-distances curves.

The red line in Fig. 4(e) corresponds to the situation where β is twice as large as for the black solid line. Similarly to Fig. 4(c), the point where F_g and F_{sc} cancel lies at a longer distance. The shift of the cancelation point is a direct manifestation of the situation where F_g increases while F_{sc} remains constant. The set point of the cantilever thus has a profound influence on the relative magnitude of the measured optical forces. Consider the two curves in Fig. 4(e), representing an object in the sample with β (black) and a second object with 2β (red). Depending on the set point of the cantilever, the contrast between these two objects may vary drastically. For the values used in this simulation, if the set point is at $\sim$15 nm the force measured at the object represented by the black curve is minimum while the net photoinduced force measured at the object with the red curve is substantial. However, if the cantilever set point is moved to 20 nm, the situation is reversed. The strongest force is now measured at the object with the weaker gradient force, as the net force at this distance is governed by F_{sc}. Hence, objects which give rise to a stronger F_g do not always produce the strongest signals in PIFM. The contrast observed is dependent on the cantilever set point. Consequently, knowledge of the force-distance curve is essential for interpreting images generated with photoinduced force microscopy.

B. Photoinduced forces near gold nanostructures

We next apply the developed formalism to experimentally obtained amplitude-distance measurements. Gold nanowires deposited on a glass surface are chosen as the test object. Figure 5 shows the amplitude (a) and phase (b) of first resonance and the amplitude of second resonance (c), which are recorded simultaneously while the tip is parked over the gold nanowire. The amplitude of the second resonance (A_2) shows the characteristic peak, followed by a shallow dip and a plateau at longer distances. At shorter tip-sample distances, A_2 settles at $\sim$195 pm, as the tip enters hard-contact mode, indicated by the blue data points. As expected, in this regime A_1 and θ_1 remain invariant. This region is relevant to photothermal force measurements [5–8].

Figure 5(d) depicts the reconstructed force from the measured amplitude and phase curves (black squares). The extracted curve shows three clear regimes. At short distances, in the hard-contact region, the force is invariant. As the set point of the cantilever is decreased, the gradient force becomes important. The observed dip corresponds to the distance where $F_g + F_{sc} = 0$. At longer distances, the scattering force dominates. Note that the force does not approach exactly zero at the dip. The observed offset is attributed to the presence of thermal noise at the mechanical frequency ω_2, resulting

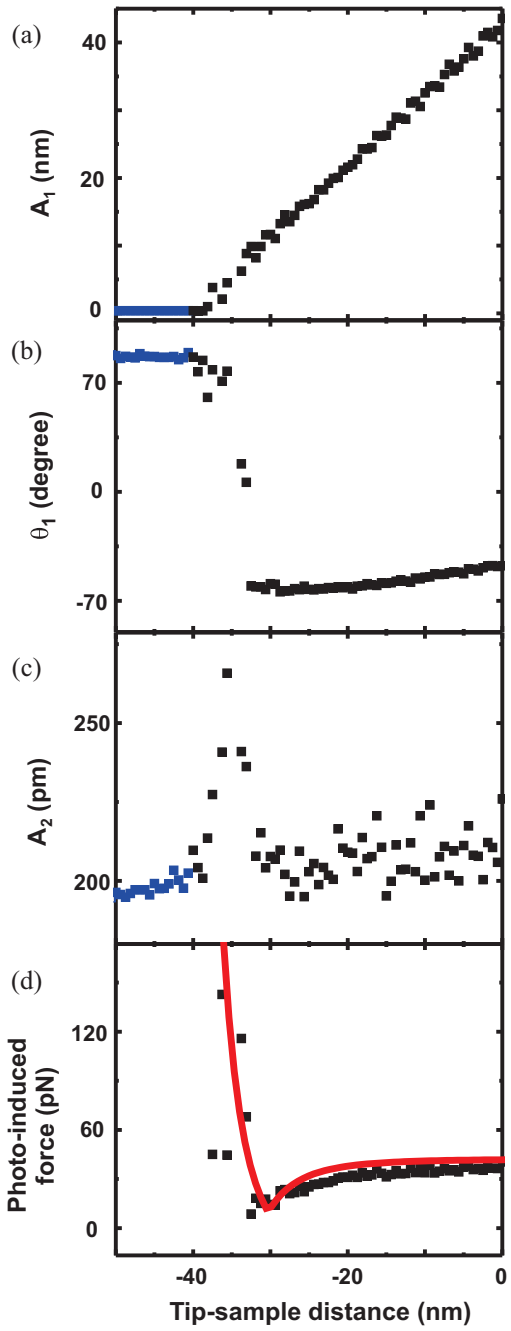

FIG. 5. (Color online) The amplitude (a) and the phase (b) of the fundamental resonance with respect to tip-sample distance on gold nanowire. The zero is the set point at which the tip is engaged. The tip is retracted from the sample. (c) The amplitude of the second resonance of the cantilever on the gold nanowire. (d) Squares represent the reconstructed experimental data from the nanowire and the red line is the model fit. Blue data points indicate the hard-contact region.

in a residual fluctuation force [24,25]. The reconstructed force curve can be fitted by Eq. (29), which is shown by the red line in Fig. 5(d). Based on the fit, an estimated value for the scattering force can be extracted as $F_{sc} =$ 32.0 pN, and gradient force prefactor β is found as 2.06×10^{-42} N m^4.

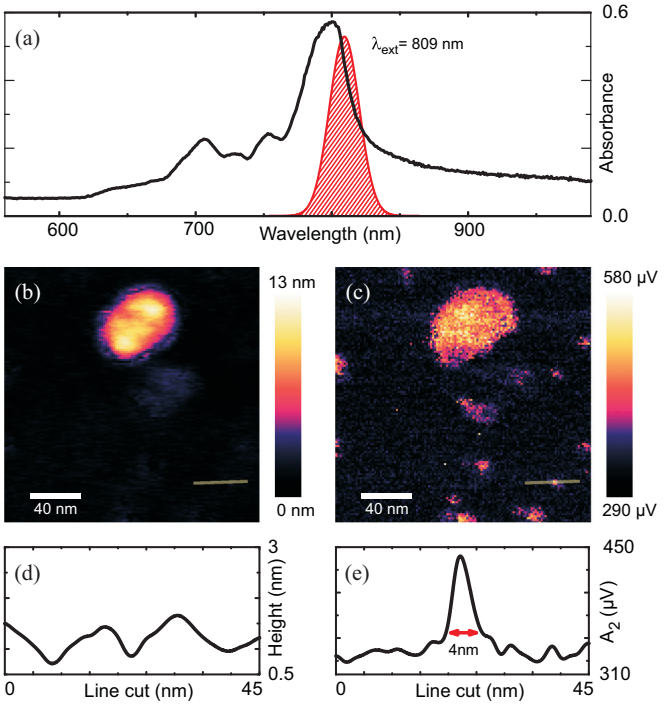

FIG. 6. (Color online) (a) Linear absorption spectrum of silicon-naphtalocyanine (SiNc). The laser spectrum is indicated by the shaded area. (b) Topography image of clusters of SiNc and (c) the corresponding photoinduced force image of SiNc. (d) One-dimensional cut at the line shown in the topography image (b). (e) One-dimensional cut at the line shown in the photoinduced force image (c).

C. Photoinduced forces and molecular resonances

We next apply PIFM with fs pulses to visualize nanoscopic clusters of molecules. The sample used in this study is silicon naphtalocyanine (SiNc) molecules deposited on a glass coverslip. SiNc displays a strong absorption at 800 nm, which significantly overlaps with the spectrum of the laser pulses used. Figure 6(b) shows the topography image of a nanoscopic cluster of SiNc molecules on the glass surface. The corresponding photoinduced force image is shown in Fig. 6(c). The PIFM image shows the same cluster as identified in the topography image. Whereas the topography image suggests height variations in the cluster, the PIFM image shows a nearly uniform signal in the cluster. This response is expected from the gradient force, which is a local force that is manifest close to the surface and relatively independent of volume effects. In addition to the larger cluster, smaller structures can be seen in Fig. 6(c) which appear absent in the topography image. The one-dimensional line cuts shown in Figs. 6(d) and 6(e) confirm that some smaller features are uniquely resolved in the photoinduced force image. The width of these structures is <10 nm, corresponding to the spatial resolution of the photoinduced force microscope. Similar structures have been seen before in photoinduced force microscopy, and have been suggested to originate from a single or a few molecules [10].

Figures 7(a) and 7(b) show the amplitude- and phase-distance curves, respectively, when the illuminated tip is positioned on the large cluster of molecules. These measurements

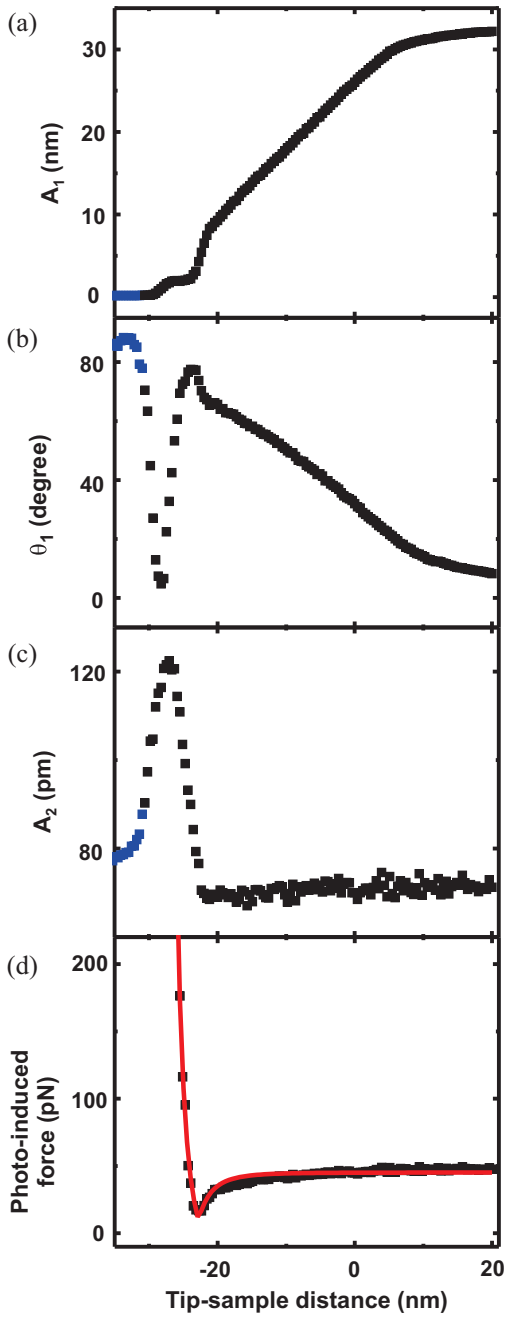

FIG. 7. (Color online) The amplitude (a) and the phase (b) of the fundamental resonance with respect to tip-sample distance on Si-naphthalocyanine (SiNc). The zero is the set point at which the tip is engaged. The sample is on the negative side. The tip is retracted from the sample. (c) The amplitude of the second resonance of the cantilever on SiNc. (d) The reconstructed optical forces on SiNc (squares) and the model fit (solid red line).

help identify the onset of tip engagement and the regime in which hard contact (blue data points) is reached. Photoinduced force measurements are performed by overlapping the laser modulation frequency with the third mechanical resonance of the cantilever at $f_{03} = 1033.190$ kHz. At this higher frequency, the effects of fluctuating thermal force contributions is expected to be reduced. The amplitude of the third mechanical

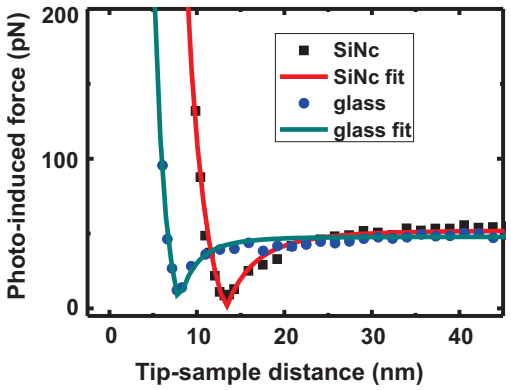

FIG. 8. (Color online) Comparison of the retrieved force-distance curves measured on SiNc and on glass.

resonance is shown in Fig. 7(c) and the extracted force is plotted in Fig. 7(d). Similar to the measurements on the gold nanowire, a clear dip can be seen in the force-distance curve, which is attributed to the cancellation of F_g and F_{sc}. Using Eq. (29), the force-distance curve can be fitted. From the fit, we find that $F_{sc} = 59.0$ pN and $\beta = 6.10 \times 10^{-43}$ N m^4. Note that the β prefactor in the SiNc measurements is smaller than in the measurements on gold, indicating that the gradient force between the tip and the SiNc is weaker than for the case of the gold nanowire.

In Fig. 8 we compare the force-distance curve measured on another SiNc cluster with the force-distance curve recorded on the glass surface adjacent to the cluster. We observe that the cancellation point between F_g and F_{sc} appears for shorter tip-sample distances on the glass surface compared to when the tip is placed over the SiNc cluster. This is a consequence of the stronger F_g measured over the molecular cluster. To cancel out the stronger attractive force, the tip has to be moved farther from the sample, yielding an apparent shift of the dip in the force-distance curve.

The hard-contact region, where thermal expansion effects are most prominently measured, is clearly identified in the measurement. Fitting of the curves yields $\beta = 1.64 \times 10^{-42}$ N m^4 for the SiNc cluster and $\beta = 1.75 \times 10^{-43}$ N m^4 for the glass surface. The stronger gradient force for the molecular cluster is expected, as the molecular resonance dresses the material with a higher polarizability than the transparent glass material. The gradient force, therefore, is a sensitive probe of the optical properties of the sample under the tip. The scattering force in both measurements, however, is comparatively similar: $F_{sc} = 52.1$ pN for the SiNc cluster and $F_{sc} = 45.3$ pN for the glass surface. Unlike the gradient force, the scattering force extends over a larger scale and is predominantly dictated by the optical response of the tip. The scattering force is relatively insensitive to the polarizability of the (molecular) sample, which is also evidenced by Eq. (13).

D. Feasibility of photoinduced force microscopy with fs pulses

Unlike previous photoinduced force experiments, which were carried out with cw illumination [10,11], the force measurements reported here are conducted with 200 fs optical pulses derived from a ti:sapphire laser. Because of the much

higher peak powers compared to cw irradiation, the use of fs pulses may raise concerns regarding optical nonlinearities at the tip that may negatively affect the stability and duration of the experiment. It is known that gold-coated tips exhibit plasmon resonances that can be driven at the excitation wavelength of 809 nm, which give rise to strong fields at the apex [26,27]. Such high fields may induce nonlinear optical photodamage of the tip's nanomorphology, which in turn affects the effective polarizability of the tip and the optical force that results from it. In addition, unfavorable heat kinetics can give rise to time-varying thermal fluctuations on the time scale of the experiment, which may overwhelm the cantilever dynamics driven by the pN photoinduced forces.

However, our experiments suggest that photoinduced force measurements can be confidently conducted with fs illumination. We find that keeping the illumination power well below 100 μW sustains stable conditions that enable force measurements over several hours. The use of a high-repetition rate laser is favorable in this regard, as a steady state in the tip-heating dynamics is achieved on the relevant time scale of the experiment. The ability to use fs pulsed excitation in optical force measurements opens exciting prospects for developing experiments where the measured force is induced by selected nonlinear optical manipulations of the sample.

V. DISCUSSION AND CONCLUSION

In this work, we have studied the mechanisms that contribute to the signals measured in photoinduced force microscopy. This new form of microscopy operates in a regime away from the hard-contact mode, as is required in IR AFM techniques. Consequently, thermal expansion of the sample after optical excitation is not the primary contrast mechanism in PIFM. Instead, the technique is directly sensitive to the electromagnetically induced forces in the tip-sample junction, as described by the gradient force F_g and the scattering force F_{sc}. PIFM enables the measurement of F_g and F_{sc}, and generates images with contrast based on the spatial variation of these two optical forces.

We have provided a theoretical description of cantilever dynamics in the presence of F_{opt}, the sum of F_g and F_{sc}. The photoinduced force is conveniently detected at modulation frequencies that coincide with higher-order resonances of the cantilever system. The amplitude of the cantilever at the frequency of the higher-order mechanical resonance reflects the competition between the attractive gradient force and the repulsive scattering force. The simulated amplitude-distance curve reveals a minimum at the tip-sample distance where F_g and F_{sc} cancel. The z-distance at which the minimum occurs may change as a function of lateral position in the sample, as the relative contributions of F_g and F_{sc} may vary from point to point. Therefore, the positive (attractive) contrast in photoinduced force microscopy is dictated by the spatial variation of F_g relative to F_{sc}.

Our formulation allows the reconstruction of the photoinduced forces from amplitude-distance measurements. Experiments on bare glass, gold nanowires, and molecular clusters confirm that F_g and F_{sc} manifest themselves on different spatial scales. Fits to the reconstructed force-distance curves indicate that F_g is local and, because of the z^{-4} dependence, significant only for tip-sample distances within a few nm. In addition, F_g is sensitive to the polarizability of the sample object. For instance, the polarizability of the glass surface at the 809 nm excitation wavelength is significantly lower than the polarizability of the optically resonant SiNc nanocluster, resulting in a much stronger measured F_g for the latter. The scattering force, on the other hand, shows no distance dependence on the nanoscale. This observation complies with the theoretical description of F_{sc} in Eq. (13), which states that it is manifest over a length scale defined by the axial extent of the optical excitation field ($\sim\mu$m).

Whereas F_g varies dramatically with the polarizability of the sample, the measurements, conducted under similar experimental conditions, reveal that F_{sc} is in the 30–60 pN range for all measurements presented here. This is to be expected from Eq. (13), which indicates that the magnitude of the scattering force is defined by the interaction of the excitation light with the tip. Naturally, the magnitude of F_{sc} is a direct function of the tip material and morphology. The different distance dependence and polarizability dependence of F_g and F_{sc} gives rise to a force-distance curve that can vary dramatically from point to point. The contrast in the image is also dependent on the set point of the cantilever. Changing the set point may change the contrast of a given object on the glass surface from positive to negative relative to the signal from the glass. This notion emphasizes that understanding the mechanisms at play in PIFM is essential for interpreting the images produced with this technique.

In short, we have theoretically and experimentally characterized the dominant forces in photoinduced force microscopy. The framework developed here makes it possible to quantitatively extract F_g and F_{sc} from photoinduced force measurements, which is essential for interpreting the image contrast. Understanding the contrast mechanism in PIFM is important for relating the photoinduced forces to molecular spectroscopic information.

ACKNOWLEDGMENTS

We thank Jonathan Burdett for his experimental help during the early stages of this project. This work was supported by the National Science Foundation, Grant No. CHE-0802913.

[1] L. Gross, F. Mohn, N. Moll, B. Schuler, A. Criado, E. Guitian, D. Pena, A. Gourdon, and G. Meyer, Science **337**, 1326 (2012).

[2] J. Zhang, P. Chen, B. Yuan, W. Ji, Z. Cheng, and X. Qiu, Science **342**, 611 (2013).

[3] L. Gross, F. Mohn, N. Moll, P. Liljeroth, and G. Meyer, Science **325**, 1110 (2009).

[4] M. Setvín, P. Mutombo, M. Ondráček, Z. Majzik, M. Svec, V. Cháb, I. Ošt'ádal, P. Sobotik, and P. Jelínek, ACS Nano **6**, 6969 (2012).

[5] A. Dazzi, R. Prazeres, F. Glotin, and J. M. Ortega, Infrared Phys. Technol. **49**, 113 (2006).
[6] A. Dazzi, C. B. Prater, Q. Hu, D. B. Chase, J. F. Rabolt, and C. Marcott, Appl. Spectrosc. **66**, 1365 (2012).
[7] A. M. Katzenmeyer, V. Aksyuk, and A. Centrone, Anal. Chem. **85**, 1972 (2013).
[8] F. Lu, M. Jin, and M. A. Belkin, Nat. Photonics **8**, 307 (2014).
[9] A. Dazzi, F. Glotin, and R. Carminati, J. Appl. Phys. **107**, 124519 (2010).
[10] I. Rajapaksa, K. Uenal, and H. K. Wickramasinghe, Appl. Phys. Lett. **97**, 073121 (2010).
[11] I. Rajapaksa, K. Uenal, and H. K. Wickramasinghe, Appl. Phys. Lett. **99**, 161103 (2011).
[12] P. Suarabh and S. Mukamel, J. Chem. Phys. **140**, 161107 (2014).
[13] L. Novotny and B. Hecht, *Principles of Nano-Optics* (Cambridge University Press, New York, 2013).
[14] R. Garcia and E. T. Herruzo, Nat. Nanotechnol. **7**, 217 (2012).
[15] J. N. Israelachvili, *Intermolecular and Surface Forces* (Academic Press, New York, 1994).
[16] B. Gotsmann, C. Seidel, B. Anczykowski, and H. Fuchs, Phys. Rev. B **60**, 11051 (1999).
[17] R. Garcia and R. Perez, Surf. Sci. Rep. **47**, 197 (2002).
[18] J. E. Sader and S. P. Jarvis, Appl. Phys. Lett. **84**, 1801 (2004).
[19] J. E. Sader, T. Uchihashi, M. J. Higgins, A. Farrell, Y. Nakayama, and S. P. Jarvis, Nanotechnology **16**, S94 (2005).
[20] M. Lee and W. Jhe, Phys. Rev. Lett. **97**, 036104 (2006).
[21] A. Bouhelier, M. Beversluis, A. Hartschuh, and L. Novotny, Phys. Rev. Lett. **90**, 013903 (2003).
[22] E. J. Menke, M. A. Thompson, C. Xiang, L. C. Yang, and R. M. Penner, Nat. Mater. **5**, 914 (2006).
[23] $f_0 = 3 \times 10^{-27}$ N m^2, $l = 2.34 \times 10^{-8}$ m, $f_0 l^4/3 = 3 \times 10^{-58}$ N m^6, $F_1 = 16 \times 10^{-11}$ N, $\beta = 5 \times 10^{-43}$ N m^4, $k_1 = 1.6$ N/m, $k_2 = 62.9$ N/m, $\omega_{01} = 60$ kHz, $\omega_{02} = 376.2$ kHz, $Q_1 = 200$, $Q_2 = 1254$, $F_{sc} = 1 \times 10^{-11}$ N.
[24] D. Kleckner and D. Bouwmeester, Nature (London) **444**, 75 (2006).
[25] J. Jahng, M. Lee, C. Stambaugh, W. Bak, and W. Jhe, Phys. Rev. A **84**, 022318 (2011).
[26] M. I. Stockman, Phys. Rev. Lett. **93**, 137404 (2004).
[27] S. Berweger, J. M. Atkin, R. L. Olmon, and M. B. Raschke, J. Phys. Chem. Lett. **3**, 945 (2012).